INSTITUTE OF PHYSICS PUBLISHING and INTERNATIONAL ATOMIC ENERGY AGENCY NUCLEAR FUSION

Nucl. Fusion **46** (2006) S933–S941 doi:10.1088/0029-5515/46/10/S10

Discrete compressional Alfvén eigenmode spectrum in tokamaks

N.N. Gorelenkov[1], E.D. Fredrickson[1], W.W. Heidbrink[2], N.A. Crocker[3], S. Kubota[3] and W.A. Peebles[3]

[1] Princeton Plasma Physics Laboratory, PO Box 451, Princeton, NJ 08543-0451, USA
[2] University of California, Irvine, California 92647, USA
[3] University of California, Los Angeles, California 90024, USA

E-mail: ngorelen@pppl.gov

Received 27 January 2006, accepted for publication 18 May 2006
Published 22 September 2006
Online at stacks.iop.org/NF/46/S933

Abstract

The spectrum of compressional Alfvén eigenmodes (CAE) is analysed and shown to be discrete in tokamaks with low aspect ratio, such as the National Spherical Torus Experiment (NSTX), as well as in conventional tokamaks, such as DIII-D. The study is focused on recent similarity experiments on NSTX and DIII-D in which sub-cyclotron frequency instabilities of CAEs were observed at similar plasma conditions (W.W. Heidbrink *et al* 2006 *Nucl. Fusion* **46** 324). The global ideal MHD code NOVA recovers the main properties of these modes predicted by theory and observed in both devices. The discrete spectrum of CAEs is characterized by three quantum mode numbers for each eigenmode, (M, S and n), where M, S and n are poloidal, radial and toroidal mode numbers, respectively. The expected mode frequency splitting corresponding to each of these mode numbers seems to be observed in experiments and is consistent with our numerical analysis. The polarization of the observed magnetic field oscillations in NSTX was measured and is also consistent with the numerical analysis, which helps to identify them as CAE activity. CAE mode structure was obtained and shown to be localized in both radial and poloidal directions with typical radial localization toward the plasma edge and poloidal localization at the low field side of the plasma cross section.

PACS numbers: 52.55.Pi, 52.55.Fa, 52.55.Qzf

(Some figures in this article are in colour only in the electronic version)

1. Introduction

The spectrum of compressional Alfvén eigenmodes (CAE) driven by a phase space gradient is measured and systematically analysed numerically in the National Spherical Torus Experiment (NSTX) and DIII-D plasmas for the first time. Multiple CAEs, if excited either internally or externally with sufficient amplitude, are expected to channel energy from fusion products or other fast ions to heat thermal ions [1, 2]. CAEs are reported to drive the plasma current in rotomak experiments [3]. CAE modes can also potentially be used for energetic particles and plasma diagnostics.

The existence of localized CAEs, also called fast Alfvén or magnetosonic eigenmodes, was initially predicted independently in two theoretical papers in cylindrical geometry [4, 5] in which it was shown that CAEs can be localized at the plasma edge for rather high poloidal mode numbers. Dispersion and polarization of these modes is consistent with the compressional Alfvén wave branch, which mode frequency is given approximately by $\omega = kv_A$, where v_A is the Alfvén velocity at the mode location and k is the characteristic wavevector. For edge localized modes $k_\theta \equiv m/r \sim k$, so that the modes propagate primarily in the poloidal direction, where m is the characteristic poloidal harmonic number and r is the minor radius of the magnetic surface. These modes and their localization were suggested to be critical in order to explain the ion cyclotron emission (ICE) from the plasma driven by superalfvenic energetic ions [6] (and in such works as [7–11]). In [12] poloidal localization of CAEs was predicted and was required for CAE instabilities to minimize their damping.

ICE was observed earlier in experiments on different tokamaks by measuring edge magnetic field oscillations with the Mirnov coils. Magnetic field spectrograms exhibited peaks of the harmonics of the fundamental cyclotron frequency of thermal ions [13–16] (and other references in a review paper [17]). Theory has predicted that the CAEs responsible for ICE should have high mode numbers and should be close in frequency so that each peak in the Mirnov spectrum near the cyclotron frequency harmonic should correspond to several instabilities. Hence, it can be understood that it was rather impossible to investigate the properties of any single CAE mode in earlier ICE experiments.

New experimental insights into the CAE physics were offered in more recent studies in the NSTX where these modes were shown to be excited in new regimes with the mode frequencies at a fraction of the thermal ion cyclotron frequency $0.3 f_{ci} < f < f_{ci}$ [18–21]. It was demonstrated that the instability frequencies correlate with the plasma Alfvén velocity, which was used to identify them as CAEs. In very recent similarity experiments between NSTX and DIII-D, CAEs were observed in DIII-D by lowering the equilibrium magnetic field to achieve the same ratio of the Alfvén velocity to the beam injection velocity [22]. Similar magnetic activity was observed in the mega ampere spherical tokamak (MAST) [23]. These recent experiments on NSTX, MAST and DIII-D renewed interest in CAE theory mainly because observed CAE spectra exhibit discrete modes well separated in frequencies due to the relatively low magnetic field used in experiments. Advanced diagnostic capabilities made it possible to measure single mode polarization and mode numbers [18, 20], which unambiguously identified observed modes to be of the compressional branch. We note that in addition to CAEs, the eigenmodes of another branch shear Alfvén called global Alfvén eigenmodes (GAEs), were seen on the magnetic spectra in the same frequency range [2]. GAEs could be easily separated from CAEs by the characteristic magnetic spectrum intersections of their signal peaks as the safety factor evolves in time, whereas the spectral lines of CAEs never intersect. Such a simple technique is supported by the analysis of the magnetic field polarization measurements.

The extension of CAE theory to low aspect ratio tokamak plasmas, such as those produced in NSTX, confirmed their radial and poloidal localization [19]. This study was done within the MHD model, whereas the extension of the model to account for the Hall term for conventional tokamaks [11, 24, 25] and STs [26] revealed the poloidal mode number sign asymmetry of the eigenfrequency and set the requirements for the plasma density to allow the CAE solution to exist. It is important to note that both radial and poloidal mode localizations were confirmed by theories with the Hall term included.

Limited numerical studies were published to confirm theoretical findings by solving the CAE envelope equations such as in [12, 25]. Most recently, global calculations with the use of the wave codes did find a localized CAE solution for the highest possible toroidal mode numbers, n (at fixed mode frequency) [27], whereas simulations did not show any localization of the CAEs at low n's. Due to numerical problems simulations were performed up to $n \sim 10$. Note that the poloidal localization of the CAEs is critical for the modes with frequencies at high harmonics of the thermal ion cyclotron frequency as it allows avoiding the cyclotron damping of these modes on bulk ions [12]. It seems to be less critical for the instabilities in NSTX, but appears to be favourable for the CAE instability because injected mostly passing beam ions interact more efficiently with such modes due to outboard radial deviation of their drift trajectories at the low field side (LFS) of the plasma cross section.

We perform a systematic numerical study of the CAE spectrum in the conventional tokamak and in the low aspect ratio tokamak ('spherical torus', ST) in order to verify theoretical predictions for the CAE dispersion and space localization. We use global ideal MHD code NOVA [28, 29], which is able to recover slow, shear and compressional Alfvén branches.

2. High frequency mode observations in NSTX and DIII-D

2.1. Summary of experimental observations in NSTX

Both edge magnetic pick-up coil and reflectometer diagnostics have observed high—up to thermal ion cyclotron frequency—coherent plasma oscillations in NSTX [18–20]. Observations showed broad and complicated frequency spectra of coherent modes between 400 kHz and up to 2.5 MHz, with the fundamental cyclotron frequency of background deuterium ions to be $f_{cD0} = \omega_{cD}/2\pi = 2.3$ MHz, calculated at the vacuum magnetic field at the geometrical axis of NSTX for $B_{g0} = 0.3$ T [18]. In experiments the Alfvén velocity was varied by controlling the magnetic field and plasma density, which resulted in a correlation with the mode frequencies. Typically the range of operational parameters for the experiments are toroidal current $I_p = 0.7$–1 MA, $B_{g0} = 0.3$–0.45 T, central electron density $n_{e0} = 1$–5×10^{13} cm^{-3}, central electron temperature of up to $T_{e0} = 1$ keV. CAEs were observed only in plasmas heated by a deuterium beam with a power of $P_b = 1.5$–3 MW. The CAE instability was shown to be very sensitive to the distribution function of the NBI ion. It was also observed that the frequency of a single unstable mode does not change during the discharge if the NBI sources with different injection angles are changed. It was concluded that CAEs in that plasma are the cavity modes, i.e. CAEs are normal modes of the plasma and can exist without fast particles. The typical magnitude of the perturbed magnetic field at the plasma edge is small $\delta B_\parallel / B \sim 10^{-6}$ [18].

2.2. New evidence for the compressional polarization of high frequency oscillations in NSTX

New capabilities of the magnetic pick-up coil Mirnov diagnostic include the possibility of measuring the mode number and the polarization of the magnetic field oscillations [20]. We show the magnetic spectrum at high frequency for NSTX discharge #117521 in figure 1 with the following plasma parameters: $B_{g0} = 0.44$ T, major radius at the geometrical centre $R_0 = 0.85$ m, minor radius of the last magnetic surface in the equatorial plane $a = 0.61$ m, $n_{e0} = 5.83 \times 10^{13}$ cm^{-3} and $f_{cD0} = 3.39$ MHz, whereas at the edge $f_{cD\text{edge}} = 2.67$ MHz. Also shown is the polarization of three particular modes measured near the plasma edge, which clearly illustrates that these modes are of the compressional branch since $\delta B_\parallel > \delta B_\perp$. Measurements of the toroidal mode number often give low- to medium-n's. In the example shown in the figure, the low band of modes at $0.5 < f[\text{MHz}] < 1$ has mostly positive low toroidal mode numbers $-1 \leqslant n < 7$, whereas the higher frequency band, $1.6 < f[\text{MHz}] < 2.2$ is characterized by rather high negative toroidal mode numbers, n changing sequentially from -9 to -13 as the mode frequency goes up. With respect to the beam ion injection direction, positive n's mean that the mode is propagating against both the plasma current and the direction of the beam injection.

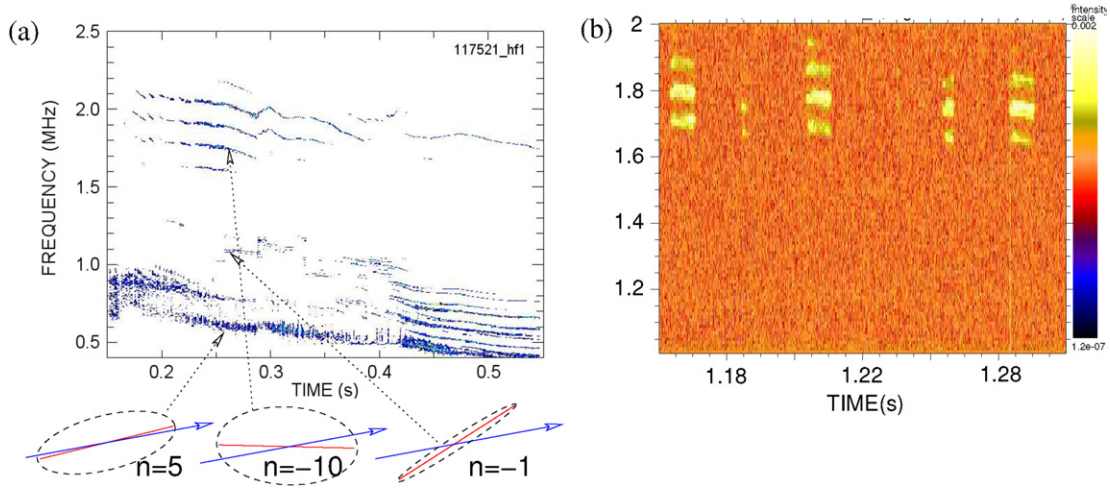

Figure 1. High frequency magnetic field oscillation spectrum evolution during NSTX discharge #117521 (*a*) and during DIII-D discharge #122806 (*b*). Shown also are the results of the polarization measurements for three compressional type oscillations in NSTX (*a*). Each polarization sub-figure has an ellipse, which is the trace of the perturbed magnetic field vector, and an arrow, which shows the direction of the equilibrium magnetic field.

Hence, we conclude that the pick-up coil measurements clearly identify the CAE modes in NSTX. We must note that few of the modes from the lower band in that figure seem to have shear Alfvèn wave polarization. Throughout the whole evolution of the spectrum the measurements of each peak polarization seems to be consistent for each mode. The shear Alfvèn branch in this frequency range is represented by the global shear Alfvèn eigenmodes, considered in [2].

2.3. CAE observations in DIII-D

In experiments on DIII-D [22] plasma conditions similar to those in NSTX were created to investigate conditions for high frequency instabilities in conventional tokamaks since the two machines have different major radii, $R_0 = 1.67$ m in DIII-D ($a = 0.61$ m). High frequency observations at $f \sim f_{ci}/2$ in conventional tokamaks were not reported before. When the magnetic field was lowered to such a value that beam ions are superalfvenic, high frequency instabilities appear with the similar properties observed in NSTX. Qualitatively, observations agree with theory, but some discrepancies remain. An example of the magnetic spectrum is shown in figure 1(*b*) for the DIII-D similarity experiment plasma shot #122806, which was chosen out of an experimental database in which both reflectometer and magnetic pick-up coils diagnostics were available and showed similar spectra. The modulation in the signal is due to the modulation in the applied beam injection. Unfortunately the identification of the toroidal mode numbers and the polarization of the measured magnetic activity was not possible within the campaign. However, the general spectra properties are similar to those in NSTX. One of them strongly suggests that the observed magnetic activity is CAE instability, which is that the CAE spectrum peaks are not intersecting in time. This is consistent with the dispersion of CAEs, $\omega = kv_A$, opposite to the shear Alfvèn branch, $\omega = k_\parallel v_A$, where $k_\parallel \sim m/qR - n/R$. It follows from here that the frequency of shear Alfvèn modes should intersect in time as q is evolving.

3. CAE modelling by MHD code NOVA

It is known that ideal MHD equations contain both shear and compressional Alfvén waves. It turns out that the problem of finding the shear branch eigenmode is rather straightforward and can be modelled both analytically and numerically by such MHD codes as NOVA, which was applied to NSTX observations of high frequency modes [2]. A compressional branch is more sensitive to the non-ideal effects such as finite ω/ω_c corrections coming from the Hall term [11, 24, 25], but nevertheless can be well studied within the ideal MHD model [4,5,12]. As we argued in the introduction the Hall term effect is well studied. It is expected to create the poloidal mode number sign asymmetry and modifies the CAE frequency, accordingly. However, it is not expected to change the mode localization [25, 26].

Let us first recall key elements contributing to the eigenmode equation for CAEs, which will help to understand the following numerical results. In the analysis hereafter we will be considering one NSTX and one DIII-D discharge with some of the plasma parameters given in section 2. Additional plasma profiles, such as the safety factor, q, and normalized plasma density, $\bar{n} \equiv n(r)/n(0)$, are shown in figure 2.

3.1. Heuristic eigenmode equation

For simplicity, allow for the wavelength to be small in comparison with the equilibrium scale lengths, which means that locally one can write the dispersion of the compressional branch in the form $\omega^2 = v_A^2 \nabla^2$, where we also implied that the plasma pressure is small and $\omega^2/\omega_{ci}^2 \ll 1$. If there is a direction of symmetry, such as along the cylinder axis or around the torus in the tokamak plasma we can write

$$\left(\nabla_\perp^2 - k_\varphi^2 + \frac{\omega^2}{v_A^2}\right)\xi = 0, \qquad (1)$$

where φ is the toroidal (symmetry) angle, the subscript $\perp$ means that the derivative operator is applied in the direction

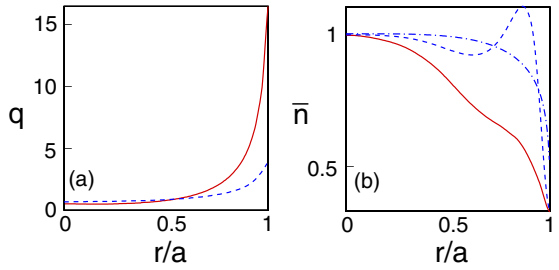

Figure 2. NSTX shot #117521, $t = 0.5$ s and DIII-D shot #122806, $t = 1.205$ safety factor (a) and normalized density (b) profiles. Solid curves correspond to NSTX plasma, whereas dashed curves correspond to DIII-D plasma. Also shown as a dash–dot curve in (b) is the monotonic model density profile used in DIII-D analysis. Safety factor values ((a)) in the centre are 0.706 and 0.982 in NSTX and DIII-D, and 16.3 and 3.02 at the edge, respectively.

perpendicular to $\nabla\varphi$, and plasma displacement ξ is chosen as the perturbed quantity. It is clear from this equation that the combination $k_\varphi^2 - \omega^2/v_A^2 \equiv V$ plays the role of an effective potential of the eigenmode problem. The variation of V in the plasma cross section perpendicular to the direction of symmetry comes from both the Alfvén velocity, $v_A^2 = B^2/4\pi\rho_{pl}$, where ρ_{pl} is the plasma mass density, and the toroidal wavevector, $k_\varphi = n/R$, where R is the major radius, and n is the toroidal mode number.

In the cylindrical geometry (limit of high aspect ratio tokamak plasma) poloidal, θ, direction is another direction of symmetry, so that the poloidal harmonic number, m, is a good quantum number for the CAE problem [4,5]. In that case the problem is reduced to solving the 1D equation in the radial direction and the effective potential is formed by the following combination $k_\theta^2 + k_\varphi^2 - \omega^2/v_A^2$, so that the plasma density and $k_\theta^2 = m^2/r^2$ radial variations form the potential well, where r is the minor radius. At sufficiently large m's and flat density profiles the well is localized toward the plasma edge. In finite aspect ratio plasma V typically has poloidal minimum at the LFS due to B poloidal variation. It is clear that if n is high, the term k_φ helps to localize the wave like region at the LFS and is argued to be the reason for poloidal localization of high-n CAEs [27]. In the opposite case of low n's, as an example, in the NSTX plasma considered in this paper, a 2D structure of potential V is shown in figure 3. When the contours of the potential is close to sufficiently elongated vertical ellipses (at high ellipticity) the problem was considered in [30]. For finite ellipticity plasma one can also expect the CAEs to be localized near the minimum of potential V.

Summarizing our heuristic theory, the frequency of CAEs is expected to be described by this equation

$$\omega_{MSn}^2 \simeq v_A^2 \left(\frac{M^2}{r^2} + \frac{S^2}{L_r^2} + \frac{n^2}{R^2} \right), \qquad (2)$$

where all relevant values should be taken at the minimum of V, S is the radial quantum number, L_r is the characteristic radial width of the effective potential, and M is the generalized poloidal quantum number, which is the same as a single poloidal harmonic number, m, only for the cylindrical geometry. In the general case the CAE solution has a single M, but should be expanded in several poloidal m harmonics.

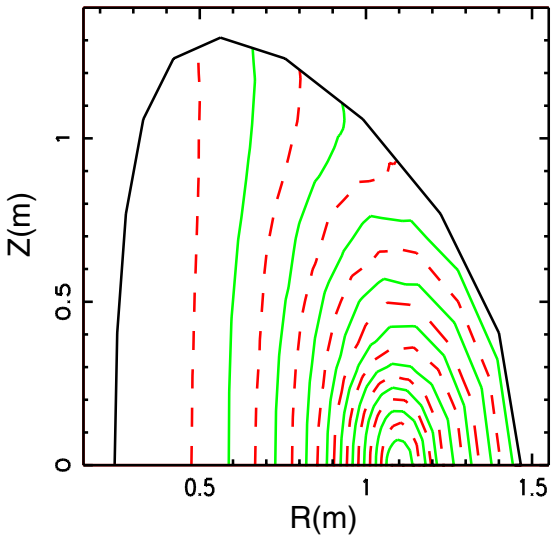

Figure 3. Effective potential V structure at $n = 0$ shown as a contour map in the poloidal cross section of the NSTX plasma. Contours correspond to the equidistant grid in V having minimum value at $Z = 0$ m, $R = 1.1$ m.

Hence, it is expected that each eigenmode corresponds to a unique combination (M, S, n).

3.2. Simulations of CAE spectrum in DIII-D plasma with model density profile

We use global ideal MHD code NOVA in realistic geometry [28,29]. It appears that in the numerical analysis low-n modes converge better than high-n modes. This is because high-n solutions typically require more than $2nq$ poloidal harmonics in the extension series. With that comes strong interaction with the Alfvèn continuum for the highest poloidal mode numbers, so that the numerical spectrum can be polluted by the singular-like solutions. In this paper we restrict our analysis to $n = 0, 1$.

As discussed in the previous section density profile determines the radial dependence of the effective potential well. Experimental density profiles in tokamaks such as the density profile from the DIII-D plasma shown in figure 2(b) are not always monotonic. Hence, we will first model the CAE spectrum with the monotonic 'model' density profile also shown in figure 2(b). NOVA employs the poloidal harmonic expansion of the solution so it is easier to compute the spectrum if it is sparse, i.e. for low mode numbers. CAE eigenfrequencies normalized to $\omega_A = v_A(0)/q_a R_0$, where q_a is the safety factor value at the edge, are shown in figure 4 for $n = 0$ as functions of M mode number. The value of M is obtained from the poloidal harmonic numbers present in the solution or from the poloidal envelope.

As one can expect, radial mode number of each mode determines the number of radial modes of the solution as shown in figure 5 and can be clearly seen from the dominant harmonics $m = \pm 1$ radial structure. Within the ideal MHD theory and for $n = 0$ modes the poloidal structure of CAE envelope is either symmetric (even) for half-integer M's ($M = 1 + 1/2,\ 2 + 1/2, \ldots$) or antisymmetric (odd) for integer M's. One can also conclude that the radial mode structure of CAEs with $S > 1/2$ is localized toward the edge, near $r/a \simeq 0.7$.

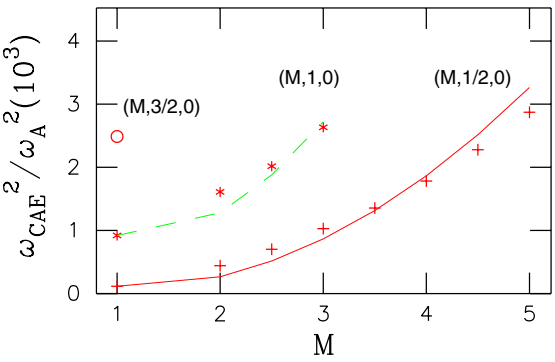

Figure 4. Computed CAE spectrum in DIII-D plasma with the model monotonic density profile. Each shown point corresponds to one solution with a given set of mode numbers (M, S, n). Shown curves correspond to heuristic quadratic dependences of M. Three bands are shown of different radial mode numbers, $S = 1/2, 1, 3/2$.

Note, that we show the plasma displacement, whereas the power of the mode should be proportional to ξ^2 and is expected to be more localized. We did not find $M = 1/2$ solution, as expected for global and poloidally periodic solutions.

CAE radial structures for the lowest radial number band, $S = 1/2$, are shown in figure 6 for different M numbers, whereas the poloidal mode structures of the same modes are given in figure 7. One can see that all modes are peaked at the LFS $\theta = 0$, which follows from figure 7(*a*) of the perturbed plasma velocity vector field and from the poloidal dependence of radial rms of the displacement (see figures 7(*b*)–(*d*)).

3.3. Simulations of CAE spectrum in DIII-D plasma with realistic density profile

The experimentally measured density profile of DIII-D plasma is non-monotonic as shown in figure 2(*b*). A noteworthy result of this is that the effective potential has two minima and two solutions with the same mode numbers and similar mode structures, but slightly different eigenfrequencies exist. Hence, the computed CAE spectrum looks more complicated as shown in figure 8, where the curves correspond to M^2 dependence for each band and at given M two solutions are shown as points marked identically (where they were found). The difference in frequency due to such 'density profile' splitting is quite small, $\Delta\omega/\omega = 1$–5%. As an example we show the structure (see figures 9(*a*) and (*b*)) of CAEs split in frequency due to this 'density profile' effect for $M = 2$, $S = 1$ and $n = 0$. As expected split modes are slightly shifted radially (in this example by $\Delta r/a \simeq 3\%$) and are somewhat differently represented by the poloidal harmonics. The normalized frequencies of these two modes are $\omega^2_{CAE}/\omega^2_A = 1.69 \times 10^3$ (figure (*a*)) and 1.85×10^3 (figure (*b*)).

Note that despite the difference in density profile, in general the spectrum from figure 8 looks similar to the one calculated for the model density profile, figure 4.

3.4. Simulations of CAE spectrum in NSTX plasma

The NSTX CAE spectrum has similar properties to the one calculated for DIII-D. This can be seen from figure 10 which also presents different radial bands. However, finding the CAE solutions for NSTX plasma turns out to be more challenging due to stronger poloidal harmonic coupling, which is a result of low aspect ratio. Within one band we observe eigenmode splitting even for the used monotonic (measured) density profile (see figure 2(*b*)). In addition, the numerically clearly identifiable lowest radial band contains several eigenmodes at given M. In fact, one can draw a second M^2 dependence curve below the solid curve shown in figure 10. This band may exist due to the geometrical effect of low aspect ratio because the effective potential is elongated vertically for which the CAE spectrum is described by theory developed in [30]. The other notable difference with the DIII-D spectrum is that in NSTX radial bands tend to be more dense in frequency for high M. In figure 11 an example of the radial and poloidal structures of $(5/2, 1, 0)$ CAE mode in NSTX is shown.

4. Comparisons with experiment and theory

4.1. Internal CAE structure comparison with the reflectometer measurements in NSTX

Reflectometer diagnostics provide an important tool to measure the internal structure of plasma oscillations and help to validate theoretical predictions. However, for robust comparison with the modelling, one needs to know both the toroidal mode number and M, which is hard to measure with present diagnostics. In the experiments on DIII-D n was not measured and only two reflectometer channels were available, so that detailed comparisons with NOVA modelling seem to be difficult. On the other hand, in NSTX not only toroidal mode numbers but the mode polarizations also were measured. Three fixed-frequency quadrature O-mode reflectometers launched microwaves into the plasma at 30, 42 and 50 GHz, which allowed for simultaneous measurements of the plasma oscillations at three radial points. Changes in the relative phase of the launched and reflected microwaves were measured and used to estimate density fluctuation levels at the cutoff making use of the phase screen model [31].

We chose the low-n mode with compressional polarization, which is persistent in time from $t = 0.25$ s to $t = 0.55$ s and is shown as having $n = -1$ in figure 1(*a*). Note that the uncertainty of the predicted toroidal mode number is approximately ± 1 measured by either the Mirnov coils or by the reflectometer. By the time of modelling $t = 0.5$ s its frequency was $f = 0.81$ MHz. Found with the NOVA code the CAE mode $(5/2, 1/2, 0)$ has the same frequency, but the mode structure turns out to be different from the measured one. The closest mode in frequency, which also reveals similar mode structure has $f = 0.93$ MHz and $(3/2, 1/2, 0)$. The results of the comparison are shown in figure 12. Note that the level of the density fluctuations is $\delta n/n \simeq 2 \times 10^{-4}$ at the peak of the reflectometer signal for this mode.

The difference in the measured mode frequency and in the calculated one can potentially point at the shortcoming of the ideal MHD model in which we ignore the Hall term. This term, as we mentioned earlier, shifts the frequency of the eigenmode depending on the sign of M number. One can see from figure 12 that the profile of the normal component of the plasma displacement and the density perturbation are quite different, which indicates that the compressional effects are critical and should be taken into account when interpreting internal measurements.

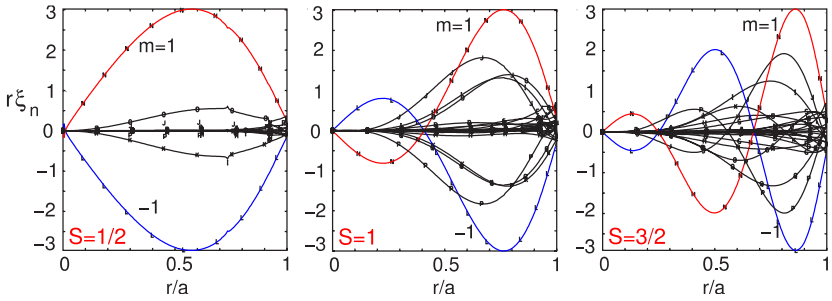

Figure 5. Expansion of CAE mode radial structures in poloidal harmonics for the lowest poloidal mode number, $M = 1$ of three radial bands, $S = 1/2, 1, 3/2$ (as marked inside figures). Shown is the normal component of the plasma displacement vector multiplied by minor radius.

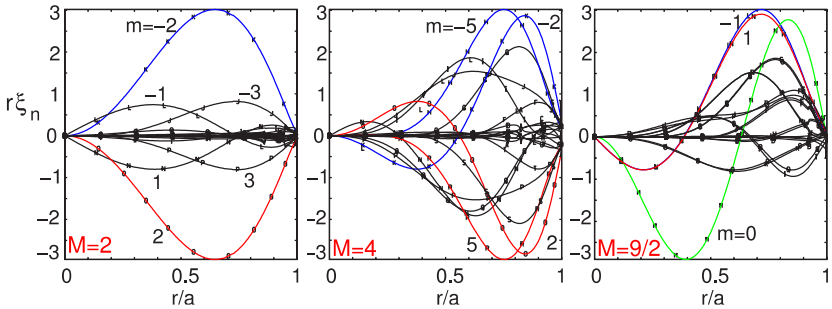

Figure 6. CAE radial structure (with notations similar to figure 5) for the first radial band, $S = 1/2$ and three poloidal numbers, $M = 2, 4, 9/2$ (as marked inside figures).

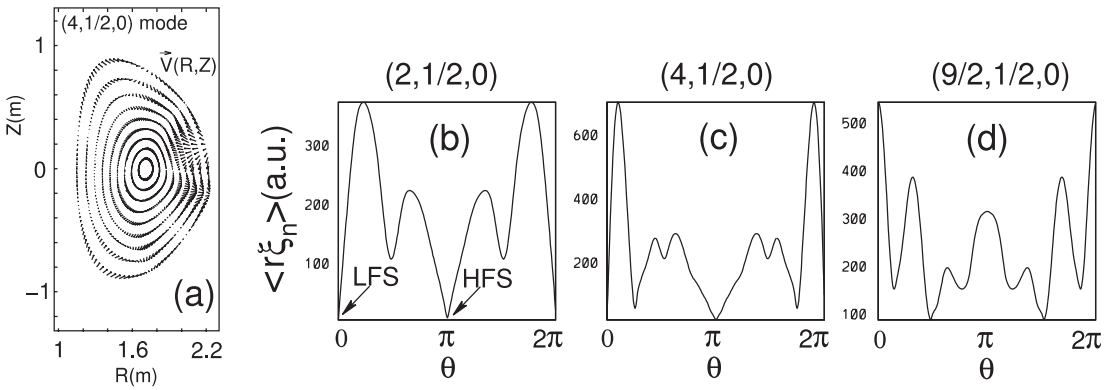

Figure 7. Perturbed velocity vector in the poloidal plane, R, Z for the mode $(4, 1/2, 0)$ (a). (b), (c) and (d) Show poloidal structure (taken as rms of the radial plasma displacement in radial direction) of CAE perturbations for the modes $(2, 1/2, 0)$, $(4, 1/2, 0)$ and $(9/2, 1/2, 0)$, respectively, which are the same modes as in figure 6.

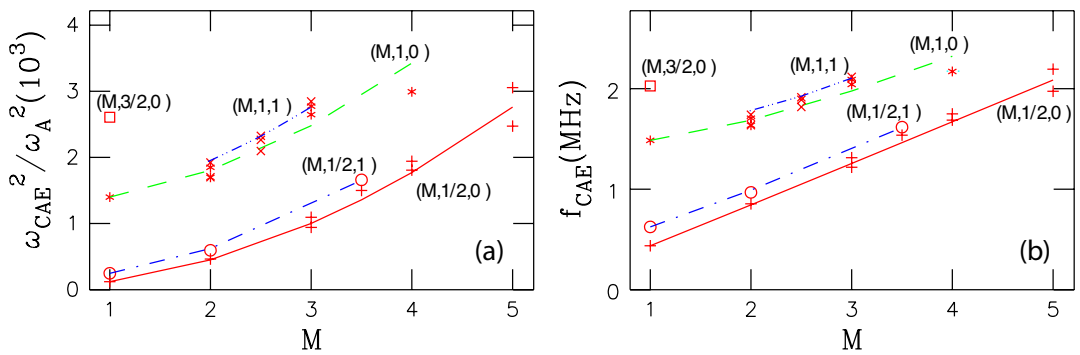

Figure 8. CAE spectrum in DIII-D computed with the realistic (non-monotonic) density profile from figure 2(b). Spectrum is shown in squared normalized frequency (a) and in frequency calculated in MHz (b). Shown are different radial bands for $n = 0$ and $n = 1$, and $S = 1/2, 1, 3/2$ as marked.

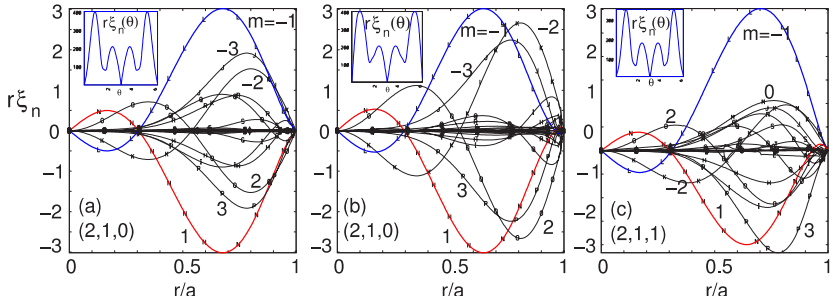

Figure 9. CAE mode structures for (2, 1, 0) mode split in two solutions, (*a*) and (*b*), due to the non-monotonic density profile shown in figure 2. (*c*) Shows the mode (2, 1, 1), which is asymmetric in sign of m due to $n \neq 0$. Insets at the top left corner of each graph show the poloidal dependence of each mode (see caption to figure 7).

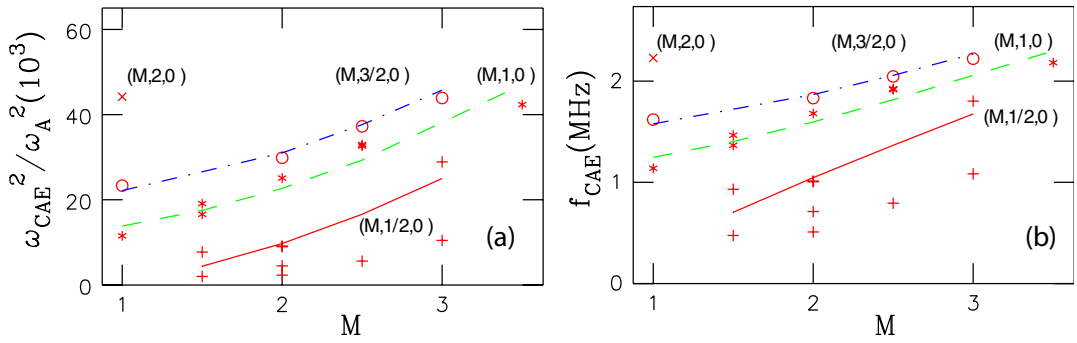

Figure 10. CAE spectrum in NSTX with the same notations as in figure 8, but only for $n = 0$, and $S = 1/2, 1, 3/2, 2$ as marked.

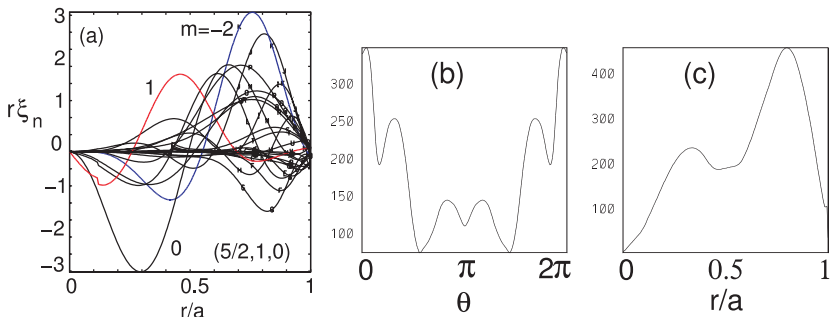

Figure 11. (5/2, 1, 0) CAE radial structure in NSTX (*a*) and its radial rms $\langle r\xi_n\rangle_r(\theta)$ (*b*) and poloidal rms $\langle r\xi_n\rangle_\theta(r)$ (*c*).

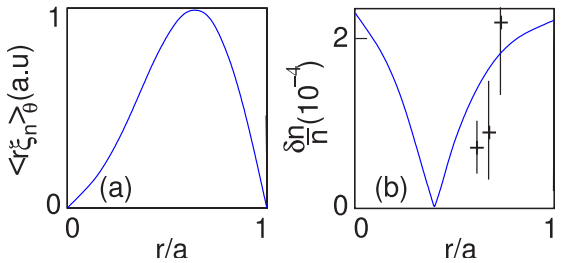

Figure 12. (3/2, 1/2, 0) CAE plasma displacement (*a*) in the midplane on the LFS in NSTX. (*b*) Shows density perturbation in the midplane. Points marked with plus signs correspond to experimental data from the reflectometer diagnostic. Shown also are the error bars for each point.

4.2. CAE frequency comparison with experiment and theory

Due to relative simplicity, frequency measurements remain one of the most important tools for studies of various plasma instabilities. Hence, it is important to compare frequency characteristics predicted by the simulations and measured in experiments.

In earlier publications on CAE observations [18, 19], it was pointed out at three characteristic frequency separations between different observed instabilities, which concluded from the data analysis and its comparison with theory. Different frequency separation scales (frequency splittings) also follow from our numerical results as presented in figures 8 and 10. They are associated with the CAE frequency variation when one of three mode numbers is changed. If we denote Δf_j to be the frequency variation due to the change in $j = M$, S or n, we can deduct from the simulated spectra that in DIII-D one expects (see figure 8(*b*)) $\Delta f_S = 0.7$–1 MHz, $\Delta f_M = 200$ kHz for $S = 1/2$, $\Delta f_M = 120$ kHz for $S = 1$, and $\Delta f_n \simeq 50$ kHz. Although the CAE spectrum in DIII-D shown in figure 1(*b*) contains only a few modes, recently reported results in similar experiments with more rich CAE spectra [22] imply the following: $\Delta f_S \simeq 1$ MHz, $\Delta f_M \simeq 130$ kHz,

Table 1. Comparison of NOVA numerical simulations, NSTX observations and theoretical predictions for CAE spectrum frequency splitting.

Splitting	NSTX experiment	NOVA	From [32]	From [26]
Radial, Δf_S	1 MHz	0.5–1 MHz	0.7 MHz	0.5 MHz
Poloidal, Δf_M	120 kHz	200 kHz	150 kHz	250 kHz
Toroidal, Δf_n	20 kHz	50 kHz	200 kHz	250 kHz

$\Delta f_n \simeq 30\,\text{kHz} \pm f_{\text{rot}}$, $f_{\text{rot}} \simeq 20\,\text{kHz}$. This seems to be in reasonable agreement with our results. A more accurate comparison does not seem possible at the moment because all three numbers have to be measured simultaneously. In addition, as we have stated earlier, the applied MHD model neglects the Hall term.

In NSTX, our simulations predict for frequency splitting $\Delta f_S = 0.5$–$1\,\text{MHz}$, $\Delta f_M = 200\,\text{kHz}$, $\Delta f_n = 50\,\text{kHz}$, whereas for the shot #117521 (figure 1(*a*)) we find $\Delta f_S \simeq 1\,\text{MHz}$, $\Delta f_M \simeq 120\,\text{kHz}$, $\Delta f_n \simeq 20\,\text{kHz} \pm f_{\text{rot}}$, $f_{\text{rot}} \simeq 20\,\text{kHz}$. Note that for the n splitting, we took the smallest frequency separation, which may also be due to the non-monotonic density profile or other geometrical effects.

A recent theoretical study of CAEs was done with the use of the Lagrangian technique [26, 32], in which a solution was sought by minimizing the corresponding functional with respect to the introduced parameters of the unknown trial function. It is expected that the results of those papers are valid in the limit of high mode numbers and, thus, only approximate agreement with our simulations can be anticipated. Table 1 summarizes the results of the frequency splitting comparison between our simulations, NSTX experiment and [26, 32]. DIII-D experimental results are similar.

The main discrepancy with theory is in the toroidal mode number splitting at low-n, and M numbers. It is surprising that the simulations are in better agreement with the simple heuristic dispersion (see equation (2)), which can be reduced to $\Delta f_n/f \sim nr^2/R^2M^2$. The poloidal mode number dependence of CAE eigenfrequency is close to the parabolic in both theories.

5. Summary

We have shown that the measurements of the magnetic field polarization help to identify unambiguously sub-cyclotron oscillations as CAEs. The ideal MHD code NOVA is capable of simulating low-n CAEs and is able to confirm poloidal and radial localization of these modes in NSTX and DIII-D predicted earlier by theory. This may be important for the development of CAE instability theory. Numerically calculated eigenmodes can be used for accurate evaluation of the CAE growth rates with such codes as NOVA-K [33].

Geometrical effects are shown to be important for the simulation of the CAE mode structure and spectrum. Simulations also show that theory qualitatively captures the main properties of CAEs. Still, some aspects such as toroidal mode number frequency splitting are not well described in analytical theory. It seems to be important to include ω/ω_c corrections in terms of the Hall term as well as the FLR effects.

We also would like to emphasize that observed CAE modes in NSTX belong to the same branch responsible for the ICE instabilities in tokamaks with higher aspect ratio, which may, however, exist at a fraction of the fundamental ion cyclotron frequency. These modes are suggested as being responsible for the anomalous energy diffusion of beam ions in TFTR experiments [34].

Acknowledgment

This work is supported by DoE contract No DE–AC02–76–CHO–3073.

References

[1] Gates D., Gorelenkov N.N. and White R.B. 2001 *Phys. Rev. Lett.* **87** 205003
[2] Gorelenkov N.N., Fredrickson E.D., Belova E., Cheng C.Z., Gates D., Kaye S. and White R.B. 2003 *Nucl. Fusion* **43** 228
[3] Petrov Y., Zhong F. and Huang T.S. 2005 *Phys. Plasmas* **12** 082514
[4] Mahajan S.M. and Ross D.W. 1983 *Phys. Fluids* **26** 2561
[5] Coppi B., Cowley S., Kulsrud R., Detragiache P. and Pegoraro F. 1986 *Phys. Fluids* **29** 4060
[6] Coppi B. 1993 *Phys. Lett.* A **172** 439
[7] Gorelenkov N.N. and Cheng C.Z. 1995 *Phys. Plasmas* **2** 1961
[8] Belikov V.S., Kolesnichenko Y.I. and Silivra O.A. 1995 *Nucl. Fusion* **35** 1603
[9] Coppi B., Penn G. and Riconda C. 1997 *Ann. Phys. (N.Y.)* **261** 117
[10] Fülöp T., Kolesnichenko Y.I., Lisak M. and Anderson D. 1997 *Nucl. Fusion* **37** 1281
[11] Kolesnichenko Y.I., Fülöp T., Lisak M. and Anderson D. 1998 *Nucl. Fusion* **38** 1871
[12] Gorelenkov N.N. and Cheng C.Z. 1995 *Nucl. Fusion* **35** 1743
[13] Greene G.J. and T. group 1990 *Proc. 17th Eur. Conf. on Controlled Fusion and Plasma Heating (Amsterdam, Netherlands, 1990)* ed G. Briffod *et al* vol 14B (Petit-Lancy, Switzerland: European Physical Society) Part IV p 1540
[14] Cottrell G.A. and Dendy R.O. 1988 *Phys. Rev. Lett* **60** 33
[15] Cottrell G.A., Bhatnagar V.P., Costa O.D., Dendy R.O., Jacquinot J., McClements K.G., McCune D.C., Nave M.F.F., Smeulders P. and Start D.F.H. 1993 *Nucl. Fusion* **33** 1365
[16] Cauffman S. and Majeski R. 1995 *Rev. Sci. Instrum.* **66** 817
[17] Heidbrink W.W. and Sadler G.J. 1994 *Nucl. Fusion* **34** 535
[18] Fredrickson E.D. *et al* 2001 *Phys. Rev. Lett.* **87** 145001
[19] Gorelenkov N.N., Cheng C.Z., Fredrickson E.D., Belova E., Gates D., Kaye S., Kramer G.J., Nazikian R. and White R.B. 2002 *Nucl. Fusion* **42** 977
[20] Fredrickson E.D., Gorelenkov N.N. and Menard J. 2004 *Phys. Plasmas* **11** 3653
[21] Gorelenkov N.N., Belova E., Berk H.L., Cheng C.Z., Fredrickson E.D., Heidbrink W.W., Kaye S. and Kramer G.J. 2004 *Phys. Plasmas* **11** 2586
[22] Heidbrink W.W., Fredrickson E.D., Gorelenkov N.N., Rhodes T. and VanZeeland M.A. 2006 *Nucl. Fusion* **46** 324
[23] Appel L.C., Akers R.J., Fülöp T., Martin R. and Pinfold T. 2004 *Proc. 31st EPS Conf. on Plasma Physics (London, UK, 2004)* ed R.M. Pick and P. Helfenstein vol 28G (CCLRC Rutherford Appleton Laboratory and Euratom/UKAEA Fusion Association Culham Laboratory: European Physical Society) P 4.195
[24] Penn G., Riconda C. and Rubini F. 1998 *Phys. Plasmas* **5** 2513
[25] Fülöp T, Lisak M., Kolesnichenko Y.I. and Anderson D. 2000 *Phys. Plasmas* **7** 1479

[26] Smith H., Fülöp T., Lisak M. and Anderson D. 2003 *Phys. Plasmas* **5** 1437
[27] Hellsten T. and Laxøaback M. 2003 *Phys. Plasmas* **10** 4371
[28] Cheng C.Z. and Chance M.S. 1986 *Phys. Fluids* **29** 3695
[29] Cheng C.Z. 1992 *Phys. Rep.* **211** 1
[30] Gorelenkova M.V. and Gorelenkov N.N. 1998 *Phys. Plasmas* **5** 4104
[31] Nazikian R., Kramer G.J. and Valeo E. 2001 *Phys. Plasmas* **8** 1840
[32] Gorelenkov N.N., Cheng C.Z. and Fredrickson E. 2002 *Phys. Plasmas* **9** 3483
[33] Gorelenkov N.N., Cheng C.Z. and Fu G.Y. 1999 *Phys. Plasmas* **6** 2802
[34] Clark D.S. and Fisch N.J. 2000 *Phys. Plasmas* **7** 2923